Nuclear energy functional with a surface-peaked effective mass: Global properties

Anthea Francesca Fantina, Jérôme Margueron, Paola Donati, Pierre M. Pizzochero

Nuclear energy functional with a surface-peaked effective mass: Global properties

A. F. Fantina[1,2], J. Margueron[1], P. Donati[2] and P. M. Pizzochero[2]
[1]Institut de Physique Nucléaire, Université Paris-Sud, IN2P3-CNRS,
F-91406 Orsay Cedex, France,
[2]Dipartimento di Fisica, Università degli Studi di Milano,
and Istituto Nazionale di Fisica Nucleare, Sezione di Milano,
Via Celoria 16, 20133 Milano, Italy

November 29, 2010

Abstract

A correction to the nuclear functional is proposed in order to improve the density of states around the Fermi surface. The induced effect of this correction is to produce a surface-peaked effective mass, whose mean value can be tuned to get closer to 1 for the states close to the Fermi energy. In this work we study the effect of the correction term on global properties of nuclei such as the density of states in ^{40}Ca and ^{208}Pb, pairing and specific heat at low temperature in ^{120}Sn. In the latter application, an explicit temperature-dependent form of the correction term is employed and it is shown that the critical temperature is reduced by 40-60 keV.

In finite nuclei, the single particle states around the Fermi energy are known to be strongly affected by the dynamical particle-hole correlations [1]. The energy of the single particle states is modified and thus the level density around the Fermi energy is changed, which in turn has an impact on low-energy properties such as pairing correlations [2,3], collective modes [4] as well as on temperature-related properties such as the entropy, the critical temperature, the specific heat [5]. In nuclear astrophysics, a good description of the density of states around the Fermi energy (which is related to the nucleon effective mass) turned out to be relevant also for the energetics of core-collapse supernovae [6, 7].

Despite the important role of the density of states in self-consistent mean field theories, most of these models such as those based on Skyrme [8], Gogny [9] and M3Y interactions [10] or on the relativistic approaches like RMF [11] or RHF [12], have a density of states around the Fermi energy that is too low. Already in the 1960s, G.E. Brown *et al.* suggested that the effective mass m^*/m should be close to 1 around the Fermi energy in order to improve the level density [13]. It could indeed be shown that the first order expansion of the energy-dependent self-energy around the Fermi surface [14,15] produces an effective mass which is the product of two different terms, the k-mass m_k and the ω-mass m_ω [1]. The ω-mass is related to the energy dependent part of the self-energy, dynamically generated by the coupling of the particles to the core-vibrations [16–19]. These dynamical correlations, which lead to an increase of the effective mass at the surface, are implemented beyond the mean field. Indeed, the effective mean field theories have an average effective mass m^*/m, the k-mass, around 0.6-0.8.

The different microscopic calculations of the particle-vibration coupling (PVC) have been performed at the first order in perturbation, due to their heavy computational features [16–22]. However, the induced effects of the PVC on the mean field itself is non-negligible. Since the effective mass is enhanced at the surface of nuclei [20], it impacts the single particle states and the pairing correlations which, in turn, modify the PVC and the effective mass. There is then a self-consistent relation between the properties of the single particle states around the Fermi energy and the PVC.

In this paper, we propose an effective short-cut for treating the effects of the PVC directly in the Energy Density Functional (EDF) approach . The coupling of the collective modes to the single particle motion induces a dynamical type of correlation that in principle could not be easily implemented in an effective nuclear interaction or in a nuclear EDF. However, the core-vibration is mainly located at the surface of the nuclei which makes the implementation in energy-density functionals easier. A parametrization of the ω-mass as a gradient of the nuclear profile has shown to give good results within a nuclear shell model [15]. In addition, the first order expansion of the self-energy near the Fermi energy induces a renormalization of the single particle Green function as well as a correction to the mean field, which almost compensate the effective component of the equivalent potential [15]. In the present approach, the surface-peaked effective mass is included through a correction term in the Skyrme energy density functional. This correction is energy independent and designed in such a way to have a moderate effect on the mean field.

The paper is organized as follows: in Sec. 1 we will describe the theoret-

ical framework. In Sec. 2 we will discuss the application to spherical nuclei, in particular, to ^{40}Ca and ^{208}Pb. In Sec. 3 we discuss the superfluid properties in connection with the surface-peaked effective mass, both at $T = 0$ and at finite temperature. Finally, in Sec. 4 we will give our conclusions and outlooks.

1 Nuclear energy density functional

The energy density functional derived from the Skyrme interaction will be considered as follows. The standard Skyrme energy-density $\mathcal{H}(\mathbf{r})$ is expressed in terms of a kinetic term $\mathcal{K}(\mathbf{r})$ and an interaction term written as [23]

$$\mathcal{H}(\mathbf{r}) = \mathcal{K}(\mathbf{r}) + \sum_{T=0,1} \mathcal{H}_T(\mathbf{r}) \ , \tag{1}$$

with:

$$\begin{aligned} \mathcal{K}(\mathbf{r}) &= \frac{\hbar^2}{2m}\tau(\mathbf{r}) \ , & (2) \\ \mathcal{H}_T(\mathbf{r}) &= C_T^{\rho}\rho_T^2(\mathbf{r}) + C_T^{\nabla^2\rho}\rho_T(\mathbf{r})\nabla^2\rho_T(\mathbf{r}) + C_T^{\tau}\rho_T(\mathbf{r})\tau_T(\mathbf{r}) \\ &+ C_T^{J}\mathbb{J}_T^2(\mathbf{r}) + C_T^{\nabla J}\rho_T(\mathbf{r})\nabla\cdot\mathbf{J}_T(\mathbf{r}) \ , & (3) \end{aligned}$$

where the kinetic density $\tau(\mathbf{r})$, the density $\rho_T(\mathbf{r})$, the spin-current $\mathbb{J}_T^2(\mathbf{r})$ and the current $\mathbf{J}(\mathbf{r})$ as well as the relation between the Skyrme parameters and the coefficients in Eq. (3) are defined in Ref. [23]. We have kept only the time-even component for the application considered in this paper. Notice the difference between the integrated energy, H, and the energy density functional, $\mathcal{H}$. These two quantities are indeed related as: $H = \int d\mathbf{r}\, \mathcal{H}(\mathbf{r})$.

In the following, we explore the impact of adding to the functional an iso-scalar correction of the form:

$$\mathcal{H}_0^{\rm corr}(\mathbf{r}) = C_0^{\tau(\nabla\rho)^2}\tau(\mathbf{r})\left(\nabla\rho(\mathbf{r})\right)^2 + C_0^{\rho^2(\nabla\rho)^2}\rho(\mathbf{r})^2\left(\nabla\rho(\mathbf{r})\right)^2 \ , \tag{4}$$

where the first term have been first introduced in Ref. [28, 29] and induces a surface-peaked effective mass while the second term is introduced to moderate the effect of the first one in the mean field.

The effective mass is obtained from the functional derivative of the energy H and is expressed as (q runs over neutrons and protons: $q = n, p$):

$$\frac{\hbar^2}{2m_q^*(\mathbf{r})} \equiv \frac{\delta H}{\delta\tau_q} = \frac{\hbar^2}{2m} + C_q^{\tau}\rho_q(\mathbf{r}) + C_0^{\tau(\nabla\rho)^2}\left(\nabla\rho(\mathbf{r})\right)^2 \ , \tag{5}$$

where the coefficient $C_q^\tau = (C_0^\tau \pm C_1^\tau)/2$ (with + for $q = n$ and − for $q = p$), and the mean field reads:

$$U_q(\mathbf{r}) = U_q^{\rm Sky}(\mathbf{r}) + U^{\rm corr}(\mathbf{r}) \ , \tag{6}$$

where $U_q^{\rm Sky}(\mathbf{r})$ is the mean field deduced from the Skyrme interaction [23] and $U^{\rm corr}(\mathbf{r})$ is the correction term induced by Eq. (4) which is defined as:

$$\begin{aligned} U^{\rm corr}(\mathbf{r}) &= -2C_0^{\tau(\nabla\rho)^2}\Big(\tau(\mathbf{r})\nabla^2\rho(\mathbf{r}) + \nabla\tau(\mathbf{r})\nabla\rho(\mathbf{r})\Big) \\ &- 2C_0^{\rho^2(\nabla\rho)^2}\Big(\rho(\mathbf{r})(\nabla\rho(\mathbf{r}))^2 + \rho(\mathbf{r})^2\nabla^2\rho(\mathbf{r})\Big) \ . \end{aligned} \tag{7}$$

From the variation of the total energy H with respect to the ground state density matrix we obtain the following set of self-consistent Kohn-Sham equations:

$$\left[-\nabla\cdot\frac{\hbar^2}{2m_q^*(\mathbf{r})}\nabla + U_q(\mathbf{r}) - iW_q(\mathbf{r})\cdot(\nabla\times\sigma)\right]\Phi_{\lambda,q}(\mathbf{r}) = \epsilon_{\lambda,q}\ \Phi_{\lambda,q}(\mathbf{r}) \ , \tag{8}$$

where λ runs over neutron and proton orbitals.

For spherical nuclei, the single particle wave functions $\Phi_{\lambda,q}$ can be factorized into a radial part and an angular part as (cf. Eq. (26) of Ref. [24]):

$$\Phi_{\lambda,q}(\mathbf{r},\sigma,\tau) = \frac{\phi_{\lambda,q}(r)}{r}\ \mathcal{Y}_{l,j,m}(\theta,\phi,\sigma)\ \chi_q(\tau) \ , \tag{9}$$

where σ is the spin and τ the isospin, and the radial wave function satisfies the following equation:

$$\left[-\frac{\hbar^2}{2m}\frac{\mathrm{d}^2}{\mathrm{d}r^2} + \frac{\hbar^2}{2m}\frac{l(l+1)}{r^2} + V_q^{\rm eq}(r,\epsilon)\right]\psi_{\lambda,q}(r) = \epsilon_{\lambda,q}\psi_{\lambda,q}(r) \ , \tag{10}$$

where $\phi_{\lambda,q}$ differs from the solution of Eq. (10), $\psi_{\lambda,q}(r)$, by a normalization factor, $\phi_{\lambda,q}(r) = (m_q^*(r)/m)^{1/2}\psi_{\lambda,q}(r)$. The equivalent potential $V_q^{\rm eq}$ is usually introduced for practical reasons,

$$V_q^{\rm eq}(r,\epsilon) = \frac{m_q^*(r)}{m}\Big[V_q(r) + U_q^{so}(r)\langle\mathbf{l}\cdot\sigma\rangle + \delta_{q,p}V_{Coul}(r)\Big] + \left[1 - \frac{m_q^*(r)}{m}\right]\epsilon_{\lambda,q} \ , \tag{11}$$

where $U_q^{so}(r)$ is the spin-orbit potential [23], V_{Coul} is the Coulomb potential, and

$$V_q(r) = U_q^{\rm Sky}(r) + U^{\rm corr}(r) + U_q^{\rm eff}(r) \ , \tag{12}$$

$$U_q^{\rm eff} = -\frac{1}{4}\frac{2m_q^*(r)}{\hbar^2}\left(\frac{\hbar^2}{2m_q^*(r)}\right)'^2 + \frac{1}{2}\left(\frac{\hbar^2}{2m_q^*(r)}\right)'' + \left(\frac{\hbar^2}{2m_q^*(r)}\right)'\frac{1}{r} \tag{13}$$

In the original work of Ma and Wambach [15], the term $U^{\rm corr}(r)$ was derived directly from the Green's function with energy dependent self-energies while, in our approach, $U^{\rm corr}(r)$ is derived from the new term (4) in the EDF. A one-to-one correspondence between EDF and the Green's function approach is not possible. However, since the terms $U^{\rm corr}(r)$ and $U_q^{\rm eff}(r)$ compensate each other in the Green's function approach [15], we want to reproduce the same behavior in the EDF. We obtain approximate compensation between $U^{\rm corr}(r)$ and $U_q^{\rm eff}(r)$ by imposing the following relation between the new coefficients:

$$C_0^{\rho^2(\nabla\rho)^2} = 12 \text{ fm } C_0^{\tau(\nabla\rho)^2} \ . \tag{14}$$

We have investigated the sensitivity of the results to the value of the proportionality constant and we have checked that the reasonable values lie in the range 10-20 fm, after which the compensation is no longer efficient.

The effects of the correction terms in (4) will be analyzed in the next section. Notice that a surface-peaked effective mass could also be obtained from a modified Skyrme interaction. This different approach potentially leads to an improved agreement with experimental single particle energies [25]. Since the new term explored in Ref. [25] is simultaneously momentum and density dependent, the functional obtained is quite different from Eq. (4): the number of terms is much larger and the correction to the effective mass is a polynomial in the density. It would be interesting to carry out a more detailed comparison of these two different approaches in a future study.

2 Mean field properties

In the following, we study the influence of the correction introduced by the new term $\mathcal{H}_0^{\rm corr}$ for two representative nuclei: ^{40}Ca and ^{208}Pb, using BSk14 interaction [26], which is adjusted to a large number of nuclei (2149). The effective mass in symmetric matter at saturation density is $0.8m$ and the isospin splitting of the effective mass in asymmetric matter qualitatively agrees with the expected behavior deduced from microscopic Brueckner-Hartree-Fock theory [27]. In the following, we study the effect of the correction term on top of BSk14 interaction without refitting the parameters. The refit is in principle necessary since the correction term impacts the masses and changes the single particle energies. In this first exploratory work, we improve the level density and discuss the effects on other quantities like the pairing, the entropy and the specific heat. The correction term (4) could

however potentially bring a better systematics in the comparison to experimental single particle centroids. This will be studied in a future work.

The neutron and proton effective masses are plotted in Fig. 1 for different values of the coefficient $C_0^{\tau(\nabla\rho)^2} = 0$, -400, -800 MeV fm^{10}. Notice that the case $C_0^{\tau(\nabla\rho)^2} = 0$ is that of the original Skyrme interaction BSk14. Increasing $|C_0^{\tau(\nabla\rho)^2}|$ from 0 to 800 MeV fm^{10}, we observe an increase of the effective mass m^*/m at the surface, which produces a peak for large values of $C_0^{\tau(\nabla\rho)^2}$, while at the center of the nucleus the effective masses get closer to the values obtained without the correction term. Fig. 1 can be compared with Fig. 1 of Ref. [15]. Due to the different surface-peaked functions (here $(\nabla\rho)^2$ instead of a single ∇ dependence in Ref. [15]), the width of the effective mass at the surface is larger in Ref. [15] than in the present work. For values of the coefficient $|C_0^{\tau(\nabla\rho)^2}|$ larger than 800 MeV fm^{10}, the potentials $U^{\rm corr}(r)$ and $U_q^{\rm eff}(r)$ (Eq. (7), (13)) induce large gradients of the mean field (12) in a tiny region close to the surface of the nuclei, which in turn produce an instability in the HF iterations.

A surface-peaked effective mass has also been deduced from the particle-vibration coupling within the HF+RPA framework [20]. In such an approach, the effective mass is shown to be peaked not only at the surface of the nuclei, but also in a window around the Fermi energy of $\pm$ 5 MeV. Such an energy dependence could not be implemented straightforwardly in the EDF framework. We could however evaluate the state-averaged effective mass, $\langle m_q^*/m\rangle_\lambda$, defined as:

$$\langle m_q^*/m\rangle_\lambda = \int d\mathbf{r}\ \phi_{\lambda,q}^*(\mathbf{r})\frac{m_q^*(\mathbf{r})}{m}\phi_{\lambda,q}(\mathbf{r})\ , \tag{15}$$

where the index λ stands for the considered state. The state-averaged effective masses $\langle m_q^*/m\rangle_\lambda$ are represented in Fig. 2 as a function of the energy of the bound states, and for different values of the parameter $C_0^{\tau(\nabla\rho)^2}$. As the value of the coefficient $|C_0^{\tau(\nabla\rho)^2}|$ gets larger, the state-averaged effective masses $\langle m_q^*/m\rangle_\lambda$ approach 1 around the Fermi energy while it get closer to the original effective mass for deeply bound states. Notice however quantitative differences between Ca and Pb for states around the Fermi energy as well as deeply bound states. In conclusion, even if we did not introduce an explicit energy dependence of the surface-peaked effective mass, we still find that the expected behavior [20] of $\langle m_q^*/m\rangle_\lambda$ as a function of energy is qualitatively reproduced.

In order to evaluate the impact of the new term on the density of states,

we display in Fig. 3 the neutron and proton number of states as a function of the excitation energy, defined as:

$$N(E) = \int_0^E dE' \; g(E') \; , \tag{16}$$

where g(E) is the density of states,

$$g(E) \equiv \frac{\mathrm{d}N(E)}{\mathrm{d}E} = \sum_{\lambda_1 < F, \lambda_2 > F} (2j_{\lambda_2} + 1) \; \delta(E - (\epsilon_{\lambda_2} - \epsilon_{\lambda_1})) \; , \tag{17}$$

and ϵ_{λ_1} (ϵ_{λ_2}) represent the single-particle energies below (above) the Fermi surface. The expected relation between the surface-peaked effective mass and the density of states is clearly shown in Fig. 3: the number of states at given excitation energy increases as the coefficient $C_0^{\tau(\nabla\rho)^2}$ goes from 0 to -800, meaning that the density of states also increases as $|C_0^{\tau(\nabla\rho)^2}|$ gets larger.

Let us now discuss qualitatively the impact of the correction term (4) on global properties of nuclei starting with the density profiles. The neutron and proton densities are shown in Fig. 4. Since for ^{40}Ca the neutron density is very similar to the proton one, we have chosen to represent only the neutron one. Since the number of particles has to be conserved, lower values of the density in the bulk of nuclei for larger values of $|C_0^{\tau(\nabla\rho)^2}|$ are compensated by a slight increase of the size of the nucleus. These small differences in the density profile influence the charge root mean square radius r_{ch} (see Table 1), which slightly increases as the value of the parameter $|C_0^{\tau(\nabla\rho)^2}|$ gets larger. Moreover, because of the isoscalar nature of the correction (4), neutrons and protons are affected in an identical way, as one can see from the constant value of the neutron skin radius, r_{skin}, given in Table 1.

Let us now analyze the influence of $\mathcal{H}_0^{\rm corr}$ at the level of the mean field $V_q(r)$ defined in Eq. (12). The different components of the central part of the mean field, $U_q^{\rm Sky}(r)$, $U_q^{\rm eff}(r)$, and $U^{\rm corr}(r)$, see Eqs. (7) and (13), are represented in Fig. 5 for the neutrons, the protons, and for ^{40}Ca and ^{208}Pb nuclei. The value of the coefficient is fixed to be $C_0^{\tau(\nabla\rho)^2} = -400$ MeV fm^{10}. As expected, there is a reasonable compensation between $U_q^{\rm eff}(r)$ and $U^{\rm corr}(r)$. As a consequence, the mean field $V_q(r)$ is nearly not affected by the presence of a surface-peaked effective mass for the values of the coefficient $C_0^{\tau(\nabla\rho)^2}$ chosen in the domain going from 0 to -800 MeV fm^{10}, except close to the surface where a small change in the slope is observed. We have then

shown that in the EDF framework, the correction term (4) reproduces the result obtained in Ref. [15].

We now compare our results to the recent ones of Zalewski *et al.* [28,29] where correction terms such as (4) as well as others have been studied. The main differences between our approach and that of Refs. [28,29] are: *(i)* the moderating term is not present in Refs. [28,29], *(ii)* the effective mass in the bulk of nuclei is close to $0.8m$ in our case, while in the Refs. [28,29] it assumes the value 1 since they started with SkX-Skyrme interaction [31] , *(iii)* we have not refitted the parameters of the interaction contrarily to Refs. [28, 29]; indeed, at variance with our approach, the functional is readjusted in Refs. [28, 29] such that the condition

$$\int d\mathbf{r}\ \frac{\rho_0(r)}{A}\ \frac{m^*(r)}{m} = 1 \tag{18}$$

is satisfied. An important dependence of the spin-orbit splitting and of the centroids as a function of the coefficient of the correction term have been observed in Ref. [28]. In our case, as shown in Figs. 6 and 7 for both ^{40}Ca and ^{208}Pb nuclei, we do not find such an important effect. Only a weak dependence on the coefficient $C_0^{\rho^2(\nabla\rho)^2}$ of the spin-orbit splitting is observed and an almost independence of the spin-orbit centroids. This contradiction between the two results might come from the readjustement of the Skyrme parameters (point *(iii)* mentioned above) performed in Ref. [29]. In the latter article, the spin-orbit interaction is not changed, but the parameters of the Skyrme interaction are changed, which might induce a modification of the density profile and, therefore, of the spin-orbit splitting. In fact, in Ref. [29] another procedure is adopted, the *non-perturbative* one, and the behavior of the the spin-orbit splitting and of the spin-orbit centroids is quite different from that shown in Ref. [28]. The *non-perturbative* prescription of Ref. [29] shows almost no change of the spin-orbit splittings and centroids with respect to the strength of the surface-peaked effective mass. This shows that the spin-orbit splittings and their centroids might not be impacted by the presence of a surface-peaked effective mass in a direct way, but eventually, indirectly, through the readjustment procedure of the functional.

Finally, we have studied how the binding energy varies as a function of the correction term (4). The results are presented in Table 2. The binding energy of ^{40}Ca and ^{208}Pb increases as the parameter $|C_0^{\tau(\nabla\rho)^2}|$ increases. We can therefore expect that the readjustment of the parameters of the Skyrme interaction shall essentially make the interaction more attractive.

3 Pairing properties

Most of the nuclei are superfluid and it could be shown that in the weak coupling limit of the BCS approximation, the pairing gap at the Fermi surface Δ_F and the pairing interaction v_{pair} are related in uniform matter through the relation [30]:

$$\Delta_F \approx 2\epsilon_F \exp[2/(N_0 v_{pair})], \tag{19}$$

where ϵ_F is the Fermi energy, $N_0 = m^* k_F/(\hbar^2\pi^2)$ is the density of states at the Fermi surface. Then a small change of the effective mass m^* can result in a substantial change of the pairing gap.

In the following, we will consider ^{120}Sn because it is an excellent candidate to study pairing correlations [23]: ^{120}Sn is spherical and only neutrons are participating to the S-wave Cooper-pairs. An accurate description of the pairing properties can be obtained already at the level of the spherical HF+BCS framework [23]. In this section, we study qualitatively the relation between the increase of the effective mass at the surface and its consequences on the pairing properties, both at zero and at finite temperature.

We adopt a density-dependent contact interaction v_{nn} given by [33]:

$$\langle k|v_{nn}|k'\rangle = v_0 g(\rho)\theta(k,k') \ , \tag{20}$$

where the strength v_0 of the pairing interaction is adjusted to obtain an average pairing gap equals to 1.3 MeV in ^{120}Sn. The factor $g(\rho)$ in Eq. (20) is a density-dependent function (see below) and $\theta(k,k')$ is the cutoff introduced to regularize the ultraviolet divergence in the gap equation. We choose for $\theta(k,k')$ the following prescription: $\theta(k,k') = 1$ if $E_k, E_{k'} < E_c$, otherwise it is smoothed out with the Gaussian function $\exp\left(-[(E_\lambda - E_c)/a]^2\right)$. Hereafter, we choose $E_c = 8$ MeV and $a = 1$ MeV. Notice that to be compatible with HFB calculations, the cutoff is implemented on the quasiparticle energy, $E_{\lambda,q} = [(\epsilon_{\lambda,q} - \mu_q)^2 + \Delta^2_{\lambda,q}]^{1/2}$, where ϵ_λ is the HF energy, μ the chemical potential, and $\Delta_{\lambda,q}$ the average pairing gap for the state λ (see Eq. (26)). The density-dependent term $g(\rho)$ is simply defined as:

$$g(\rho) = 1 - \eta\frac{\rho}{\rho_0} \ , \tag{21}$$

where η designates the volume ($\eta = 0$), mixed ($\eta = 0.5$), or surface ($\eta = 1$) character of the interaction and $\rho_0 = 0.16$ fm^{-3} is the saturation density of symmetric nuclear matter. The isoscalar particle density, $\rho = \rho_n + \rho_p$, is defined as:

$$\rho_q(r) = \frac{1}{4\pi}\sum_\lambda (2j_\lambda + 1)\left[v^2_{\lambda,q}(1 - f_{\lambda,q}) + u^2_{\lambda,q} f_{\lambda,q}\right]|\phi_{\lambda,q}(r)|^2 \ , \tag{22}$$

where the $u_{\lambda,q}$ and the $v_{\lambda,q}$ are variational parameters. The $v^2_{\lambda,q}$ represent the probabilities that a pairing state is occupied in a state (λ, q), $u^2_{\lambda,q} = 1 - v^2_{\lambda,q}$, and $f_{\lambda,q}$ is the Fermi function for the quasiparticle energy $E_{\lambda,q}$ [34]:

$$f_{\lambda,q} = \frac{1}{1 + e^{E_{\lambda,q}/k_B T}} \ , \tag{23}$$

where k_B is the Boltzmann constant.
The local pairing field is then given by:

$$\Delta_q(r) = \frac{v_0}{2} \ g(\rho)\tilde{\rho}_q(r) \ , \tag{24}$$

where $\tilde{\rho}_q$ is the abnormal density defined as:

$$\tilde{\rho}_q(r) = -\frac{1}{4\pi} \sum_{\lambda} (2j_\lambda + 1) u_{\lambda,q} v_{\lambda,q} (1 - 2f_{\lambda,q}) |\phi_{\lambda,q}(r)|^2 \ . \tag{25}$$

The Eq. (24) is the self-consistent gap equation that should be solved consistently with the particle conservation equation (22). The average pairing gap for the state λ used in the definition of the cutoff is defined as:

$$\Delta_{\lambda,q} = \int d\mathbf{r} |\phi_{\lambda,q}(r)|^2 \Delta_q(r). \tag{26}$$

In the HF+BCS framework, Eqs. (22) and (24) are solved at each iteration. The number of iterations performed depends on the convergence of the pairing gap equation (24); it goes from about 200 up to about 1000 near the critical temperature.

3.1 Pairing properties at $T = 0$

In the following, we study the influence of the correction term (4) on the pairing properties at $T = 0$. A realistic calculation for nuclei shall treat consistently the pairing interaction in the particle-particle channel and that in the particle-hole channel. The bare interaction in the particle-particle channel shall then be replaced by the induced one which accounts for a 50% correction [35]. It is however not our intention in the present work to investigate this question. We want, at a simpler level, to clarify the role of the correction term (4) on the pairing properties, and we will show that there is indeed a correlation in space between the enhancement of the effective mass and that of the probability distribution of the Cooper pairs.

In order to reproduce the value of the average gap $\tilde{\Delta}_n = 1.3$ MeV in ^{120}Sn, we have adjusted Eq. (24) for three kinds of pairing interactions (volume, mixed, and surface), for the functional without the correction term (4). We obtain for the values (η, v_0): (0; -259 MeV fm^3), (0.5; -391 MeV fm^3), (1; -800 MeV fm^3). In Table 3 we report the values for the average neutron pairing gap $\tilde{\Delta}_n$, calculated as the average gap over the abnormal density,

$$\tilde{\Delta}_n \equiv \frac{1}{\tilde{N}} \int d\mathbf{r}\ \tilde{\rho}_n(\mathbf{r}) \Delta_n(\mathbf{r}) \ , \tag{27}$$

where $\tilde{N} = \int d\mathbf{r}\ \tilde{\rho}_n(\mathbf{r})$, and for several values of the coefficient $C_0^{\tau(\nabla\rho)^2}$. In Table 3, it is shown that the effect of the correction term (4) on the pairing gap is non-negligible. The pairing gap is increased by 200 to 700 keV as the coefficient $|C_0^{\tau(\nabla\rho)^2}|$ gets larger. An important dependence with respect to the kind of the pairing interaction (volume, mixed, surface) is also observed. The largest effect of the correction term (4) is obtained for the surface pairing gap. From the results presented in Table 3 we notice that the correction term (4) in the functional has an important influence on the average pairing gap.

In order to study the effect of the correction term on the pairing properties in a more realistic case, we have chosen to renormalize the pairing interaction, for each value of the coefficient $C_0^{\tau(\nabla\rho)^2}$, in such a way to get always at zero temperature $\tilde{\Delta}_n = 1.3$ MeV. We obtain, at $T = 0$, for $C_0^{\tau(\nabla\rho)^2} = -400$ MeV fm^{10}, the values (η, v_0): (0; -248 MeV fm^3), (0.5; -362 MeV fm^3), (1; -670 MeV fm^3), and, for $C_0^{\tau(\nabla\rho)^2} = -800$ MeV fm^{10}, the values (η, v_0): (0; -235 MeV fm^3), (0.5; -337 MeV fm^3), (1; -593 MeV fm^3). We represent in Fig. 8 the pairing field and the probability distribution of Cooper-pairs defined as

$$p(r) = -4\pi r^2 \tilde{\rho}(r) \ , \tag{28}$$

versus the radial coordinate for different values of the parameter $C_0^{\tau(\nabla\rho)^2}$. On the left panels, we display the pairing field profiles, which do not change very much with the coefficient $C_0^{\tau(\nabla\rho)^2}$; this is due to our renormalization procedure, which requires the average pairing gap to be 1.3 MeV. The right panels of Fig. 8 clearly show the correlation in space between the enhancement of the effective mass and that of the probability distribution of the Cooper pairs, i.e. the enhancement of the probability distribution is located where the effective mass is surface-peaked.

In conclusion, it has been shown in this section that the effect of the surface-peaked effective mass on the pairing properties is non-negligible.

As for approaches where the pairing interaction is empirically adjusted on some nuclei, we absorbed this effect through a renormalization of the pairing interaction. For non empirical approaches where the pairing interaction is not adjusted on nuclei properties but directly to that of the bare $^1S_0$ potential [36–40], the enhancement of the average pairing gap induced by the surface-peaked effective mass shall be treated consistently with the induced pairing interaction [35].

3.2 Pairing properties at finite temperature

The density of states around the Fermi energy shall influence the temperature-related quantities such as the entropy and the specific heat [5], and at the same time the density of states is also affected by the temperature [6,42,43]. We explore the effect of the new term on ^{120}Sn in the framework of HF+BCS at finite temperature, using the pairing interaction where the strength has been renormalized at $T = 0$ for each value of the coefficient $C_0^{\tau(\nabla\rho)^2}$. In Fig. 9 we show the neutron pairing gap as a function of temperature, for the three different kinds of pairing interactions (volume, mixed, surface). The results on the left are obtained keeping the coefficient $C_0^{\tau(\nabla\rho)^2}$ constant, while, on the right, we plot the results obtained letting $C_0^{\tau(\nabla\rho)^2}$ vary exponentially with temperature, according to the following relation:

$$C_0^{\tau(\nabla\rho)^2}(T) = C_0^{\tau(\nabla\rho)^2} \times e^{-T/T_0} \ , \tag{29}$$

with $T_0 = 2$ MeV. The choice of this kind of temperature dependence relies on the work by Donati *et al.* [6], where a study of the ω-mass in the framework of QRPA for temperatures up to some MeV was carried out on some neutron rich nuclei. The variation of m_ω with respect to temperature was parameterized with an exponential profile and the typical scale of the variation of m_ω with temperature was found to be around 2 MeV. Notice that in semi-infinite nuclear matter, the typical scale was found to be 1.1 MeV [43]. The reduction of the scale might be due to the semi-infinite model which is still far from a realistic finite nucleus case.

We observe in all cases in Fig. 9 the typical behavior associated to the existence of a critical temperature T_c after which pairing correlations are destroyed [34]. In particular, as expected, T_c is not modified by the new term for the case of constant coefficient, since we absorbed the effect of the new term through the renormalization procedure. Instead, the effect of a temperature dependent coefficient $C_0^{\tau(\nabla\rho)^2}(T)$ is to reduce the critical temperature; indeed, the chosen dependence (29) shifts the critical temperature

of ~ 40 keV in the case of volume interaction and of ~ 60 keV in the case of surface interaction. The relation $T_c \simeq \tilde{\Delta}_n(T=0)/2$ is still verified; more precisely, the ratio $T_c/\tilde{\Delta}_n(T=0)$ is $\simeq 0.55$ (for volume interaction) and $\simeq 0.57$ (for surface interaction) for the case of T-independent $C_0^{\tau(\nabla\rho)^2}$, while with the T-dependent prescription (29) it varies from $\simeq 0.55$ (for volume interaction) to $\simeq 0.51$ (for surface interaction). In conclusion, we remark that through its temperature dependence, the surface-peaked effective mass has an effect on the critical temperature, that could also be extracted experimentally [44, 45]. This perspective motivates the application of the present work to realistic cases at finite temperature.

Finally, in Fig. 10 we show the total entropy and specific heat as a function of temperature for volume and surface interaction, and for three values of $C_0^{\tau(\nabla\rho)^2}$ (0, -800 MeV fm^{10}, and $C_0^{\tau(\nabla\rho)^2}(T)$ for the case -800 MeV fm^{10}). The entropy of the system is calculated as: $S_{tot} = S_n + S_p$, being:

$$S_q = -k_B \sum_\lambda \left[f_{\lambda,q} \ln(f_{\lambda,q}) + (1 - f_{\lambda,q}) \ln(1 - f_{\lambda,q}) \right] , \tag{30}$$

where $f_{\lambda,q}$ is defined as in Eq. (23). The specific heat is then defined as:

$$C_V = T \, \frac{\partial S_{tot}}{\partial T} . \tag{31}$$

We observe the change of the slope in the entropy curve, which causes the discontinuity in the specific heat in correspondence of the critical temperature. In agreement with the previous results, T_c is shown to be modified by a temperature-dependent $C_0^{\tau(\nabla\rho)^2}$, the effect is stronger in the case of surface interaction, and the temperature dependent coefficient acts as to reduce T_c.

4 Conclusions

In this paper we have studied the influence of the correction term (4) on various nuclear properties. The isoscalar correction term (4) has been shown to produce a surface-peaked effective mass in the nuclei under study (^{40}Ca and ^{208}Pb), without modifying significantly the mean field profiles. The increase of m^*/m at the surface is up to about 1.2 - 1.3 for the maximum value of the strength of the correction we used. As the effective mass gets enhanced at the surface of nuclei, the density of states increases. Then, we have studied the impact of such a term on the neutron pairing gap in the semi-magic nucleus ^{120}Sn, within an HF+BCS framework, and it turned out

that its effect is non-negligible; if the pairing interaction is not renormalized consistently with the new term, the average gap increases from 200 keV to 700 keV under variation of the strength of the correction term and depending on the volume/surface character of the interaction. In a recent work [46], it has been stressed that the surface enhancement of the pairing field induced by the PVC might also play a role on the size of the Cooper-pairs at the surface of nuclei. In uniform matter, the coherence length is indeed inversely proportional to the pairing gap. The surface enhancement of the pairing field could then make the Cooper-pairs smaller at the surface of nuclei. It would be interesting to investigate whether this interesting feature of the pairing correlation might be probed experimentally, for example by pair transfer reaction mechanism. Finally, we have explored some finite temperature properties in ^{120}Sn, within a HF+BCS framework at finite temperature. We observed for the neutron pairing gap that the critical temperature at which pairing correlations vanish is shifted if a T-dependence in the new coefficient is considered. As a consequence, the entropy and specific heat profiles are affected by the introduction of the new term.

In the future, we shall go on with a global refitting of all the parameters of the functional, including the new correction term (4). It would be very instructive to know whether both the masses and the single particle levels could be improved in such a way.

A. F. F. and J. M. would like to thank E. Khan and N. Sandulescu for their help in checking our HF+BCS results, as well as the fruitful discussions with N. Van Giai and M. Grasso. This work was supported by CompStar, a Research Networking Programm of the European Science Foundation, by the ANR NExEN, and by the exchanged fellowship program of the Université Paris-Sud XI.

References

[1] C. Mahaux, P. F. Bortignon, R. A. Broglia, and C. H. Dasso 1985 *Phys. Rep.* **120**, 1 ; C. Mahaux and R. Sartor 1992 *Phys. Rep.* **211**, 53

[2] D. J. Dean, and M. Hjorth-Jensen 2003 *Rev. Mod. Phys.* **75**, 607

[3] Y. Satoshi, and H. Sagawa 2008 *Phys. Rev.* **C 77**, 054308

[4] M. N. Harakeh, and A. Van der Woude 2001 *Giant Resonances* Oxford Studies in Nuclear Physics

[5] N. Chamel, J. Margueron, and E. Khan 2009 *Phys. Rev.* **C 79**, 012801(R)

[6] P. Donati, P. M. Pizzochero, P. F. Bortignon, and R. A. Broglia 1994 *Phys. Rev. Lett.* **72**, 2835

[7] A. Fantina, P. Donati, and P. M. Pizzochero 2009 *Phys. Lett.* **B 676**, 140

[8] T. H. R. Skyrme 1956 *Phil. Mag.* **1**, 1043

[9] J.-F. Berger, M. Girod, and D. Gogny 1991 *Comp. Phys. Comm.* **63**, 365

[10] H. Nakada 2003 *Phys. Rev.* **C 68**, 014316

[11] B. D. Serot, and J. D. Walecka 1997 *Int. J. Mod. Phys.* **E 6**, 515

[12] W.-H. Long, N. Van Giai, and J. Meng 2006 *Phys. Lett.* **B 640**, 150

[13] G. E. Brown, J. H. Gunn, and P. Gould 1963 *Nucl. Phys.* **46**, 598

[14] A. B. Migdal 1967 *Theory of finite Fermi systems and applications to atomic nuclei*, Interscience Publishers, New York

[15] Z. Y. Ma, and J. Wambach 1983 *Nucl. Phys.* **A 402**, 275

[16] G. F. Bertsch, and T. T. Kuo 1968 *Nucl. Phys.* **A 112**, 204

[17] V. Bernard, and N. Van Giai 1979 *Nucl. Phys.* **A 327**, 397 ; V. Bernard and N. Van Giai 1980 *Nucl. Phys.* **A 348**, 75

[18] G. E. Brown, J. S. Dehesa, and J. Speth 1979 *Nucl. Phys.* **A 330**, 290

[19] P. F. Bortignon, and C.H. Dasso 1987 *Phys. Lett.* **B 189**, 381

[20] N. Van Giai, and P. Van Thieu 1983 *Phys. Lett.* **B 126**, 421

[21] E. Litvinova, P. Ring, and V. Tselyaev 2007 *Phys. Rev.* **C 75**, 064308 ; P. Ring, and E. Litvinova 2009 *ArXiv:0909.1276 [nucl-th]*

[22] K. Yoshida 2009 *Phys. Rev.* **C 79**, 054303

[23] M. Bender, P. H. Heenen, and P. G. Reinhard 2003 *Rev. Mod. Phys.* **75**, 121

[24] D. Vautherin, and D. M. Brink 1972 *Phys. Rev.* **C 5**, 626

[25] M. Farine, J. M. Pearson, and F. Tondeur 2001 *Nucl. Phys.* **A 696**, 396

[26] S. Goriely, M. Samyn, and J. M. Pearson 2007 *Phys. Rev.* **C 75**, 064312

[27] E. N. E. van Dalen, C. Fuchs, and A. Faessler 2005 *Phys. Rev. Lett.* **95**, 022302

[28] M. Zalewski, P. Olbratowski, and W. Satula 2010 Int. J. Mod. Phys. **E 19**, 794

[29] M. Zalewski, P. Olbratowski, and W. Satula 2010 *Phys. Rev.* **C 81**, 044314

[30] U. Lombardo 1999 International Review of Nuclear Physics, vol 8, Edited by M. Baldo, World Scientific.

[31] B. A. Brown 1998 *Phys. Rev.* **C 58**, 220

[32] A. M. Oros 1996 Ph.D. thesis, University of Cologne

[33] E. Garrido, P. Sarriguren, E. Moya de Guerra, and P. Schuck 1999 *Phys. Rev.* **C 60**, 064312

[34] A. L. Goodman 1981 *Nucl. Phys.* **A 352**, 30

[35] G. Gori, F. Ramponi, F. Barranco, P. F. Bortignon, R. A. Broglia, G. Colò, and E. Vigezzi 2005 Phys. Rev. **C 72**, 011302(R)

[36] T. Lesinski, T. Duguet, K. Bennaceur, and J. Meyer 2009 *Eur. Phys. J.* **A 40**, 121

[37] K. Hebeler, T. Duguet, T. Lesinski, and A. Schwenk 2009 *Phys. Rev.* **C 80**, 044321

[38] J. Margueron, H. Sagawa, and K. Hagino 2007 *Phys. Rev.* **C 76**, 064316

[39] J. Margueron, H. Sagawa, and K. Hagino 2008 *Phys. Rev.* **C 77**, 054309

[40] C. A. Bertulani, H. F. Lü, and H. Sagawa 2009 *Phys. Rev.* **C 80**, 027303

[41] M. Prakash, J. Wambach, and Z. Y. Ma 1983 *Phys. Lett.* **B 128**, 141

[42] N. Vinh Mau and D. Vautherin 1985 *Nucl. Phys.* **A 445**, 245

[43] N. Giovanardi, P. F. Bortignon, R. A. Broglia, and W. Huang 1996 *Phys. Rev. Lett.* **77**, 24

[44] M. Guttormsen, M. Hjorth-Jensen, E. Melby, J. Rekstad, A. Schiller, and S. Siem 2001 *Phys. Rev.* **C 64**, 034319

[45] A. Schiller, *et al.* 2001 *Phys. Rev.* **C 63**, 021306(R)

[46] M. Baldo, U. Lombardo, S. S. Pankratov, E. E. Saperstein 2010 *J. Phys.* **G 37**, 064016

Table 1: Charge rms radius, $r_{\rm ch}$, and neutron skin radius, $r_{\rm skin}$, for ^{40}Ca and ^{208}Pb and for different values of the coefficient $C_0^{\tau(\nabla\rho)^2}$. The charge rms radius is calculated according to Eq. (110) in Ref. [23].

	^{40}Ca		^{208}Pb	
$C_0^{\tau(\nabla\rho)^2}$ [MeVfm^{10}]	$r_{\rm ch}$ [fm]	$r_{\rm skin}$ [fm]	$r_{\rm ch}$ [fm]	$r_{\rm skin}$ [fm]
0	4.01	-0.04	6.05	0.16
-200	4.05	-0.04	6.08	0.16
-400	4.08	-0.04	6.10	0.16
-600	4.10	-0.04	6.12	0.16
-800	4.10	-0.04	6.12	0.16

Table 2: Binding energy per nucleon in ^{40}Ca and ^{208}Pb (in MeV) for different values of the coefficient $C_0^{\tau(\nabla\rho)^2}$.

$C_0^{\tau(\nabla\rho)^2}$	^{40}Ca	^{208}Pb
0	-8.781	-8.071
-200	-8.591	-7.983
-400	-8.442	-7.910
-600	-8.322	-7.849
-800	-8.227	-7.801

Table 3: Average neutron pairing gap $\tilde{\Delta}_n$ for ^{120}Sn for different values of the coefficient $C_0^{\tau(\nabla\rho)^2}$.

$C_0^{\tau(\nabla\rho)^2}$		η	
[MeV fm^{10}]	0	0.5	1
0	1.30	1.30	1.30
-200	1.33	1.36	1.47
-400	1.37	1.43	1.62
-600	1.42	1.52	1.79
-800	1.49	1.60	1.96

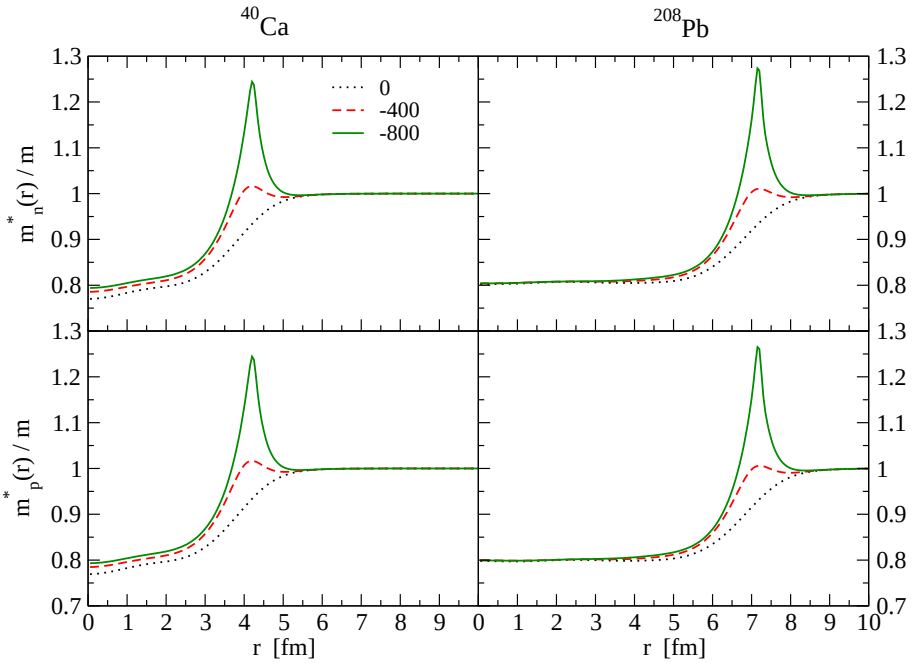

Figure 1: m_q^*/m as a function of radial coordinate for ^{40}Ca and ^{208}Pb, for $C_0^{\tau(\nabla\rho)^2}$ = 0, -400, -800 MeV fm^{10}.

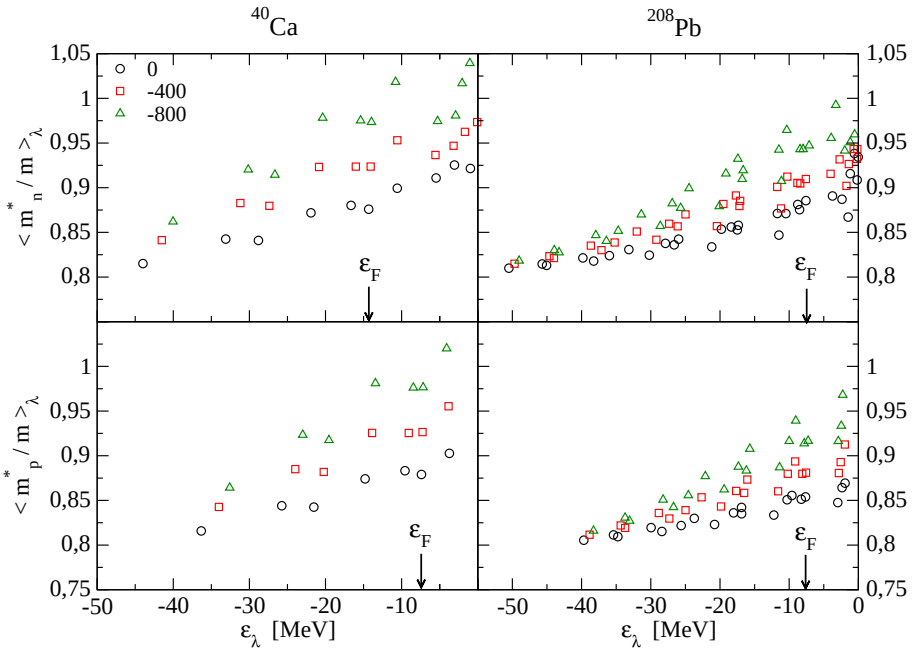

Figure 2: Energy dependence of the expectation value of $\langle m_q^*/m \rangle_\lambda$ for bound states for ^{40}Ca and ^{208}Pb, for $C_0^{\tau(\nabla\rho)^2} = 0$, -400, -800 MeV fm^{10}. The arrows indicate the position of the Fermi energy for $C_0^{\tau(\nabla\rho)^2} = 0$ MeV fm^{10} defined as the energy of the last occupied state. The correction induced by the surface-peaked effective mass produces an increase of the Fermi energy by 400 keV at most.

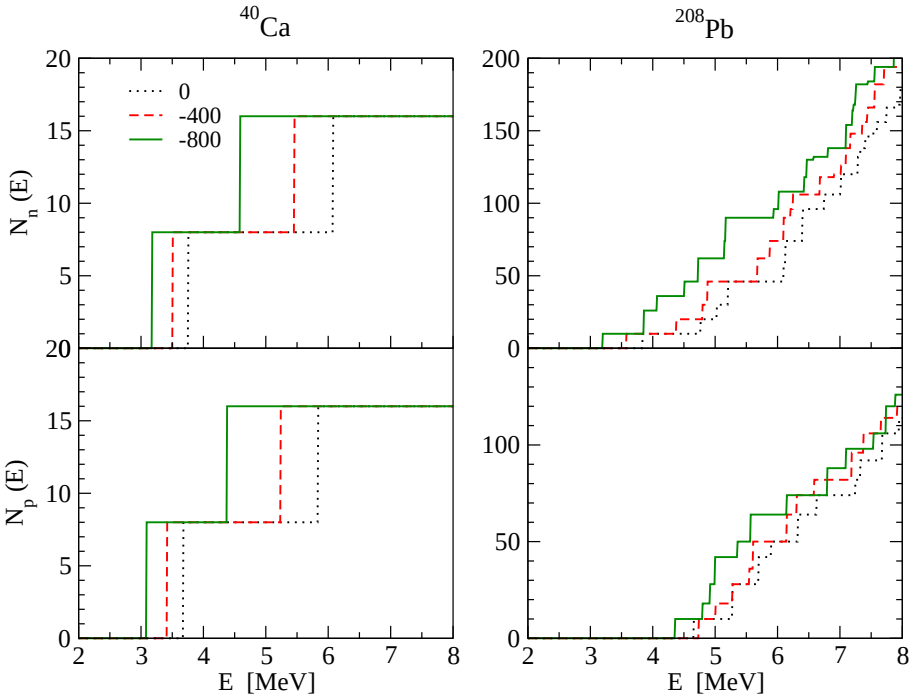

Figure 3: Number of states as a function of the excitation energy for ^{40}Ca and ^{208}Pb, for $C_0^{\tau(\nabla\rho)^2} = 0$, -400, -800 MeV fm^{10}.

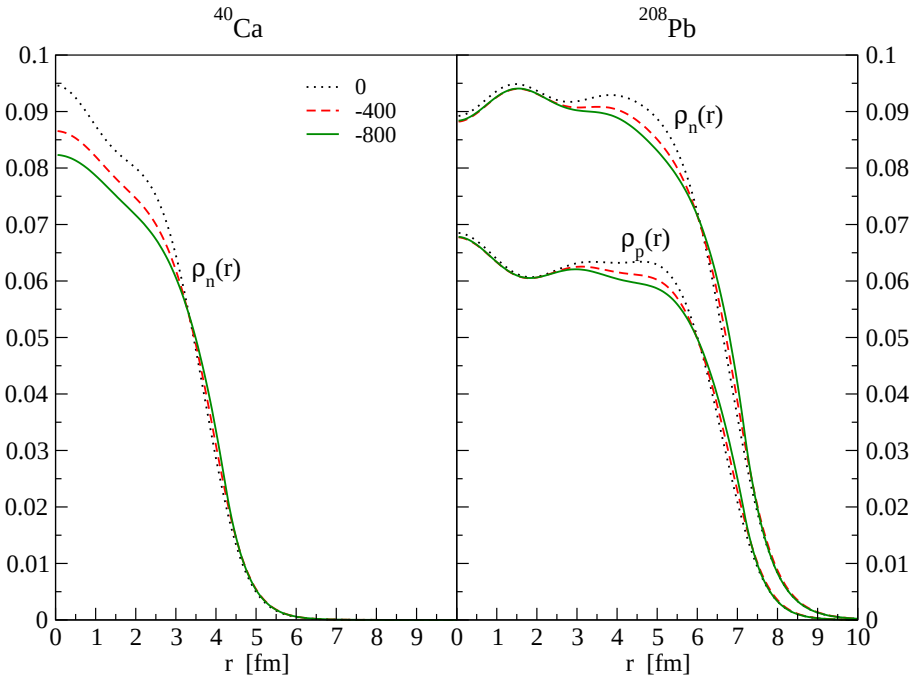

Figure 4: Neutron density as a function of radial coordinate for ^{40}Ca and neutron and proton densities as a function of the radial coordinate for ^{208}Pb, for $C_0^{\tau(\nabla\rho)^2} = 0$, -400, -800 MeV fm^{10}.

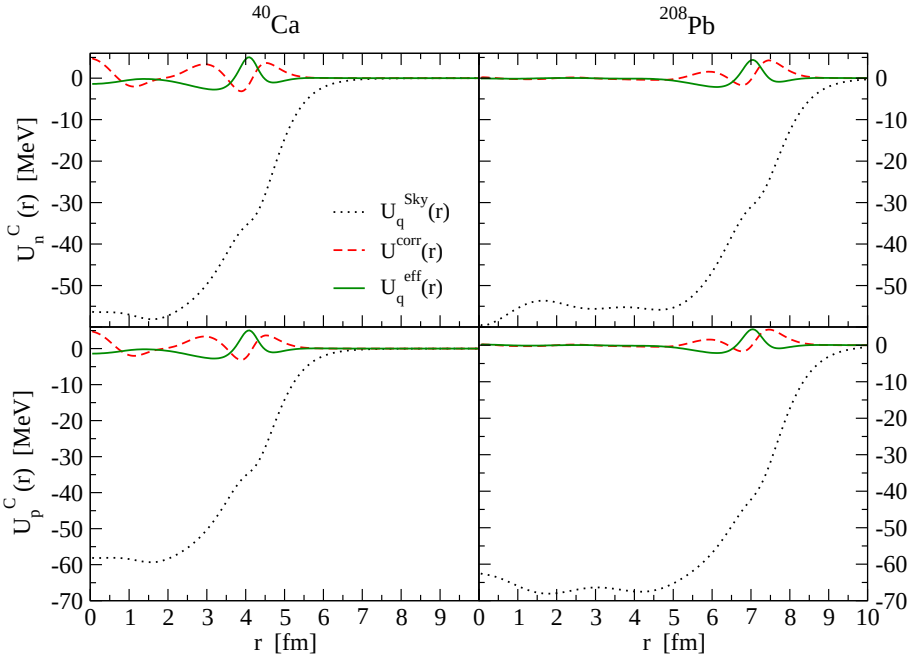

Figure 5: Central part of the neutron and proton mean field as a function of radial coordinate for ^{40}Ca and ^{208}Pb, for $C_0^{\tau(\nabla\rho)^2} = -400$ MeV fm^{10}.

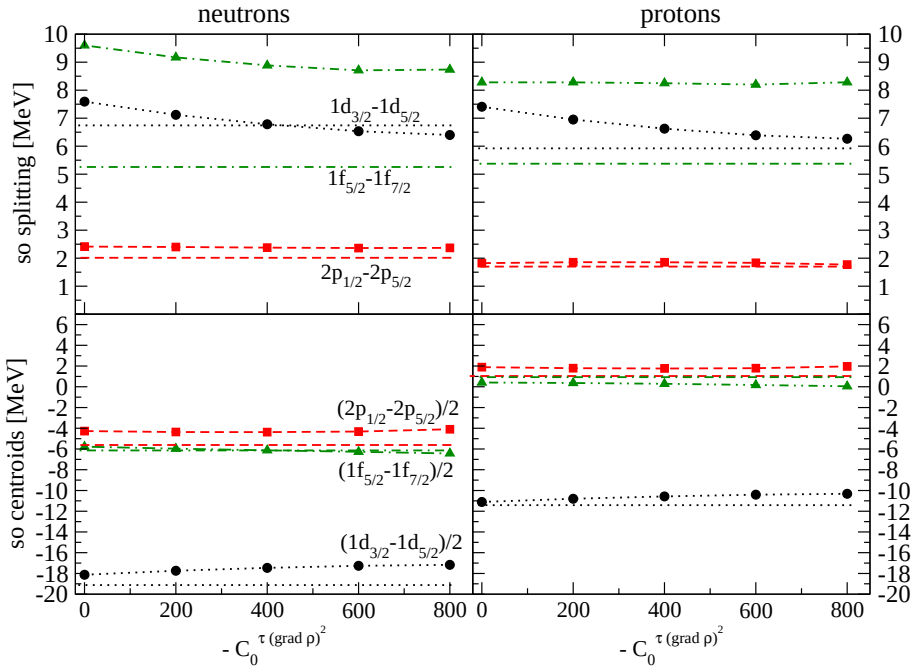

Figure 6: Spin-orbit splitting and centroids for ^{40}Ca as a function of the coefficient $C_0^{\tau(\nabla\rho)^2}$. The experimental values are taken from [32].

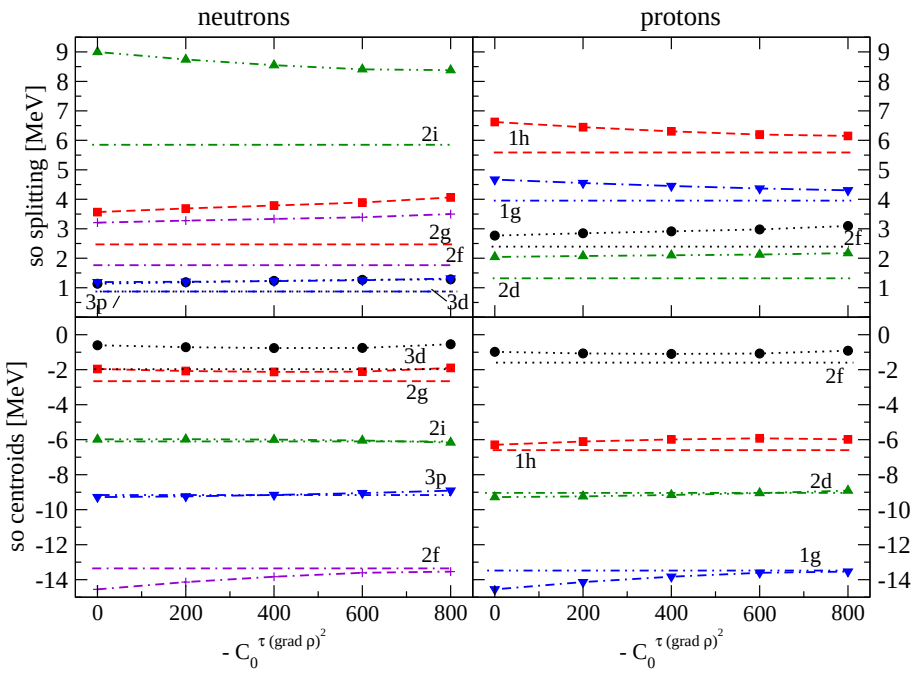

Figure 7: Spin-orbit splitting and centroids for ^{208}Pb as a function of the coefficient $C_0^{\tau(\nabla\rho)^2}$. The experimental values are taken from [24].

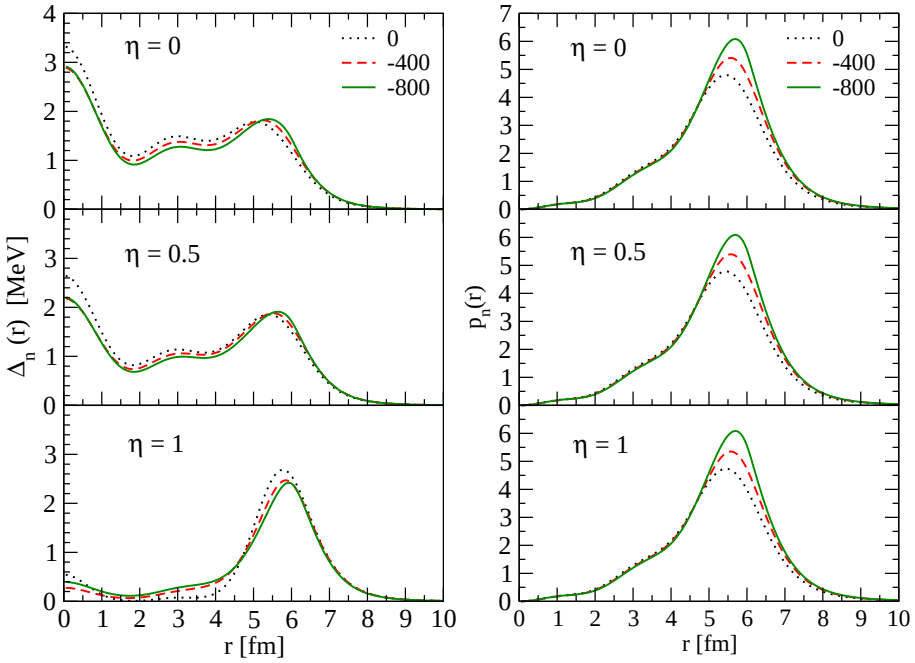

Figure 8: Neutron pairing gap (on the left) and probability distribution of the Cooper pairs (on the right) for ^{120}Sn as a function of radial coordinate, for $C_0^{\tau(\nabla\rho)^2}$ = 0, -400, -800 MeV fm^{10}, and for different types of pairing interaction (volume, mixed, surface).

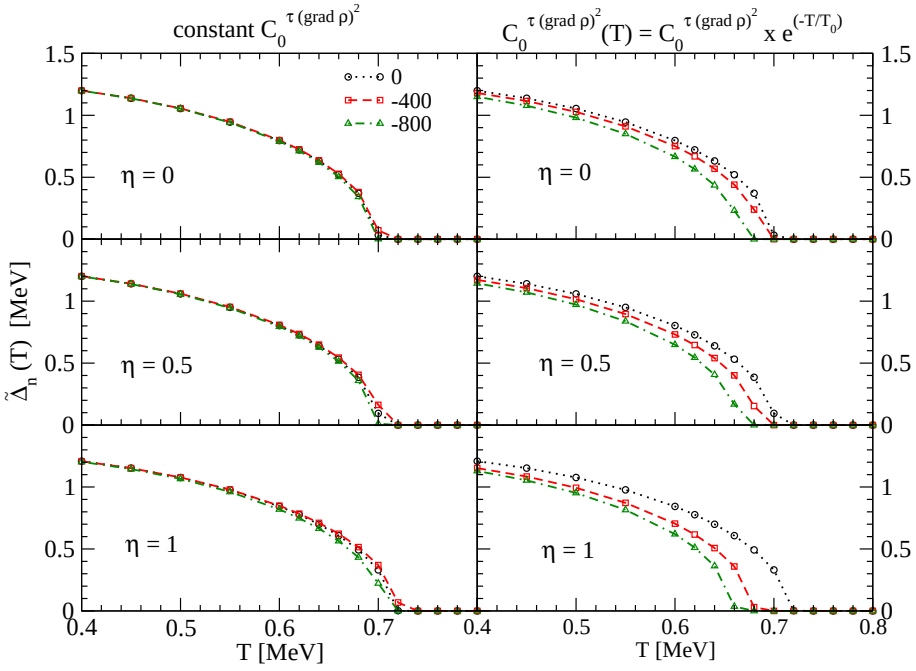

Figure 9: Neutron pairing gap for ^{120}Sn as a function of temperature for different values of the coefficient $C_0^{\tau(\nabla\rho)^2}$. The results on the left are obtained keeping $C_0^{\tau(\nabla\rho)^2}$ constant ($C_0^{\tau(\nabla\rho)^2}$ = 0, -400, -800 MeV fm^{10}), while the results on the right are obtained using for $C_0^{\tau(\nabla\rho)^2}$ the prescription in Eq. (29).

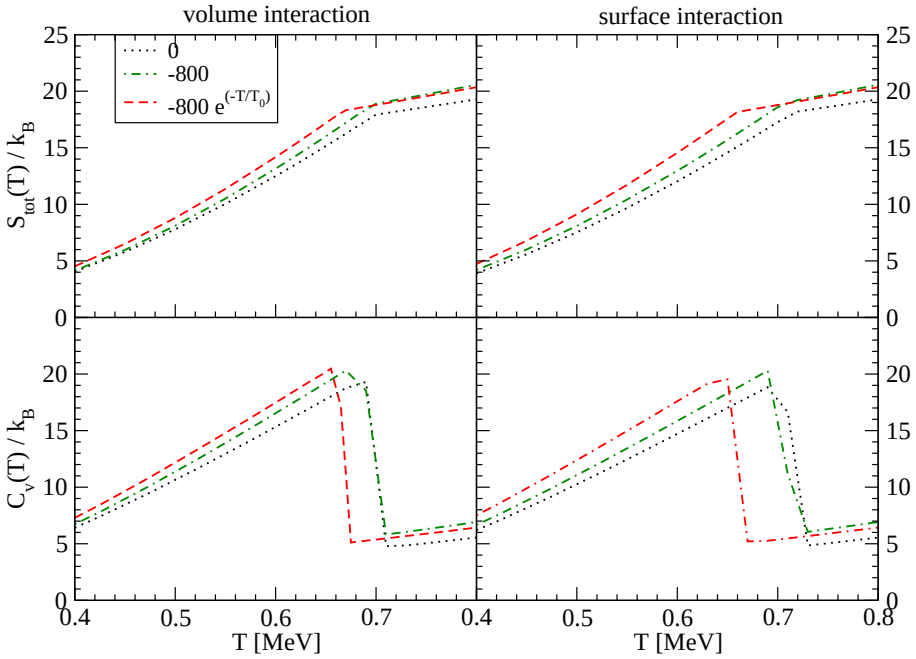

Figure 10: Total entropy S_{tot} and specific heat C_V (in units of the Boltzmann constant), for ^{120}Sn as a function of temperature, for $C_0^{\tau(\nabla\rho)^2} = 0$, -800 MeV fm^{10}, -800 e^{-T/T_0} MeV fm^{10}, and for volume (on the left) and surface (on the right) pairing interaction.